The adaptive response to long term nitrogen starvation in *Escherichia coli* requires the breakdown of allantoin

Amy Switzer, Lynn Burchell, Josh McQuail and Sivaramesh Wigneshweraraj[1]*

[1]MRC Centre for Molecular Bacteriology and Infection, Imperial College London, London, SW7 2AZ, UK

*Corresponding author: E-mail: s.r.wig@imperial.ac.uk; Tel.: +44 207 594 1867.

ABSTRACT

Bacteria initially respond to conditions that attenuate their growth by eliciting large-scale transcriptional changes. The accompanying changes in gene expression and metabolism allow the bacterial cells to effectively adapt to the growth attenuated state. How the transcriptome subsequently changes as growth attenuation ensues is not well understood. We used nitrogen (N) starvation as a model nutrient starvation condition to study the transcriptome of growth attenuated *Escherichia coli*. The results reveal that the transcriptome of nitrogen starvation-induced growth attenuated *E. coli* remains dynamic and perturbations to it compromise the viability of growth attenuated bacteria and their ability to effectively recover growth when N starvation conditions become alleviated. We further reveal that, over time, N starvation-induced growth attenuated bacteria rely on the degradation of allantoin for optimal growth recovery when N becomes replenished. This study provides insights into the temporally coordinated adaptive responses that occur in *E. coli* experiencing sustained N starvation.

IMPORTANCE

Bacteria in their natural environments seldom encounter conditions that support continuous growth. Hence, many bacteria spend the majority of their time in states of little or no growth due to starvation of essential nutrients. To cope with prolonged periods of nutrient starvation, bacteria have evolved several strategies, primarily manifesting themselves through changes in how the information in their genes is accessed. How these coping strategies change over time under nutrient starvation is not well understood and this knowledge is not only important to broaden our understanding of bacterial cell function, but also to potentially find ways to manage harmful bacteria. This study provides insights into how nitrogen starved *Escherichia coli* bacteria rely on different genes during long term nitrogen starvation.

KEYWORDS

Escherichia coli, nitrogen regulation, bacterial stress response, transcriptome, allantoin

INTRODUCTION

The process of RNA synthesis, transcription, is often the first decision-making and regulatory point in the flow of genetic information and is catalysed by the multisubunit enzyme, RNA polymerase (RNAP). The transcriptional responses that establish and maintain specific cellular states are dynamic and this plasticity is often controlled by many transcription regulatory factors that communicate with and influence the activity of the RNAP. Conditions that sustain constant bacterial growth are seldom found in nature. Whether in a host or the environment, bacteria frequently encounter nutrient deprivation, which can attenuate bacterial growth. Hence, the growth attenuated state is now widely acknowledged as an important physiological state in bacterial cell function. However, although the transcriptional basis of *bacterial growth* is widely studied, our understanding of the transcriptome of growth attenuated bacteria remains in its infancy. In fact, several recent studies on different bacteria have revealed that growth attenuated bacteria are transcriptionally active. For example: Gefen et al showed that a batch culture of *E. coli* cells retain transcriptional activity in the stationary phase of growth over a period of nearly 2 days (1); Stapels et al showed that non-growing intracellular *Salmonella* in host macrophages are transcriptionally active and this activity is important to shape the host environment to benefit bacterial survival (2); similarly, non-replicating *Mycobacterium tuberculosis* cells retained transcriptional activity in the lungs of mice (3); and more recently, Gray et al reported that *Bacillus subtilis* cells under oligotrophic conditions are transcriptionally active and replicate at an extremely slow rate (4). Therefore, understanding the transcriptional landscape in growth attenuated bacteria is important as this knowledge could inform and inspire new antibacterial strategies, such as disrupting genetic networks and

76 products that are activated during growth attenuation, which subsequently become essential for
77 survival and/or optimal growth recovery.

78 In this study, we used nitrogen (N) starvation as a model condition to understand how
79 the transcriptional landscape in nutrient starvation-induced growth attenuated *E. coli* affects
80 bacterial survival and ability to recover growth when nutrients (i.e. N) become replenished.
81 Nitrogen (N) is an integral nutrient to bacterial cell function since N is an essential element of
82 most macromolecules in the bacterial cell (proteins, metabolites, nucleic acids and cell wall
83 components). Therefore, an exponentially growing batch culture of *E. coli* rapidly becomes
84 growth attenuated upon N run-out. The initial adaptive response to N run-out, the N regulation
85 (Ntr) stress response, results in the large scale and multilevel reprogramming of the
86 transcriptome, involving ~40% of all *E. coli* genes, to allow *E. coli* to adjust to N starvation.
87 Since *E. coli* perceive N run-out as a decrease in the internal concentration of glutamine, the
88 genes expressed as part of the Ntr response are predominantly involved in the transport and
89 assimilation of nitrogenous compounds into glutamine or glutamate, yielding these
90 catabolically or sparing the requirement for them in cellular processes (5, 6). However,
91 although our understanding of the initial adaptive transcriptional response to N starvation is
92 well established, how the transcriptome changes as N starvation-induced growth attenuation
93 (NSIGA) ensues is far from clear.

94

95 **RESULTS AND DISCUSSION**

96 **Perturbation of the transcriptional response during NSIGA compromises survival**
97 **and growth recovery of *E. coli*.** To setup an experimental system to study how the
98 transcriptome changes during NSIGA, we grew a batch culture of *E. coli* in a defined minimal
99 growth medium in the presence of a limiting amount (3 mM) of ammonium chloride as the sole
100 N source (5). Under these conditions, when ammonium chloride runs out, bacteria enter a

101 complete state of N starvation, and subsequent growth attenuation (5). From the onset of N
102 starvation (N-), the viability of the population of growth attenuated *E. coli*, as measured by the
103 number of colony forming units (c.f.u.) in the population, increases at a slow rate over the
104 initial 24 h under N starvation (doubling time ~39 h, which is ~80-fold less than during
105 exponential growth when N is abundant; N+) (Fig. 1A, dark orange area). However, as N
106 starvation ensues beyond 24 h (N-24), the population ceases growth before the number of
107 viable cells gradually begins to decline after 48 h under N starvation (Fig. 1A, light orange
108 area). Thus, it seems that 24 h following N run-out, which we refer to as the N starved adaptive
109 phase (NAP), represents an important period in which metabolic processes, including
110 transcription, are temporally adjusted in order to balance maintenance of growth (albeit at a
111 very slow rate) and maximising chances of survival and growth recovery when N starvation
112 stress is alleviated.

113 To evaluate the importance of the transcriptional changes that occur during the NAP,
114 we determined how perturbation of the transcriptome during the NAP affects cell survival and
115 growth recovery when N starvation stress is alleviated. To do this, we treated the bacteria with
116 the bacteriostatic antibiotic rifamycin (Rif) at ~1 h following N run-out (i.e. N-1) for ~23 h.
117 Rif was used at 150 μg/ml as, under our experimental conditions, this concentration of Rif
118 prevents transcription elongation by the RNAP by trapping it at promoters (5). We initially
119 compared the proportion of viable cells in the Rif treated and untreated population of bacteria
120 at N-24 (i.e. ~23 h following Rif treatment at N-1). As shown in Fig. 1B, at N-24, only ~50%
121 cells in the Rif treated culture were viable compared to the Rif untreated culture. In control
122 experiments, the addition of the same amount of Rif (150 μg/ml) to bacteria at N+ (i.e. during
123 exponential growth when N was available) did not affect cell viability. This suggests that ~150
124 μg/ml of Rif is not bactericidal under our experimental conditions and that the reduction in
125 viability of the Rif treated population during the NAP in Fig. 1B is due to Rif-induced

126 perturbations to the transcriptome during the NAP. In other words, Rif-induced perturbation of
127 the transcriptional changes during NAP has a detrimental effect on cell viability. Rif treatment
128 also had a profound effect on the ability of bacteria from N-24 to resume growth compared to
129 untreated bacteria: as shown in Fig. 1C and 1D, the lag time to growth recovery of the Rif
130 treated bacteria (following c.f.u. correction to ensure an equal number of viable treated and
131 untreated bacteria were used; Fig. 1B) from N-24 was delayed by ~4.8 h compared to untreated
132 bacteria. To discount the possibility that the difference in lag time between Rif treated and
133 untreated bacteria was due to the presence of a subpopulation of bacteria that resumed growth
134 heterogeneously, we measured the lag time distribution of appearance of individual colonies
135 during growth recovery using ScanLag (7). As shown in Fig. 1E, no heterogeneity in the
136 populations of Rif treated and untreated bacteria from N-24 was detected. Further, the ScanLag
137 data also substantiates the data in Fig. 1C and 1D and demonstrates that Rif treated cells have
138 an increased lag time to growth recovery compared to untreated cells. Although, once growth
139 resumed, the doubling time of Rif treated and untreated bacteria did not markedly differ (Fig.
140 1D). Overall, we conclude that perturbation of the transcriptome during the NAP has a
141 detrimental effect on the ability of *E. coli* experiencing NSIGA to maximise chances of
142 viability and optimal growth recovery when N becomes available.
143
144 **The transcriptome *E. coli* in the NAP is dynamic.** To study the transcriptional
145 changes that occur during the NAP, we compared the transcriptomes of *E. coli* during
146 exponential growth (N+), following initial N run-out (N-), and at N-24. We defined
147 differentially expressed genes as those with expression levels changed ≥ 2-fold with a false
148 discovery rate adjusted P-value < 0.05. As previously reported by us and others, the initial
149 transcriptional response to N starvation involves differential expression of 1787 genes
150 primarily required for scavenging and catabolism of alternative N sources (6, 8, 9) and thus,

151 we did not investigate these genes further (Phase A in Fig. 2A). However, during the NAP,
152 upon transition from N- to N-24 (Phase B in Fig. 2A), 451 genes (~10% of *E. coli* genes) are
153 differentially expressed, of which 105 genes (~2% of *E. coli* genes) become differentially
154 expressed in Phase B, that were not differentially expressed in Phase A (Fig. 2B). Functional
155 categorisation of the genes uniquely differentially expressed in Phase B, hereafter called NAP
156 genes, revealed that they are involved in diverse processes including transcription, amino acid
157 transport, metabolism and several genes of unknown function (Fig. 2C). Eleven (*abgR*, *bfd*,
158 *ileY*, *leuO*, *ompN*, *sibE*, *tauA*, *ycaD*, *yedL*, *yhdV*, and *yihO*) of the upregulated and nine (*evgA*,
159 *glnA*, *gltI*, *hemH*, *ivy*, *pfkB*, *ybjX*, *yieP*, and *yjeJ*) of the downregulated NAP genes were known
160 to be regulated by either NtrC (*glnA* and *gltI*) or Nac (all other genes listed above) (9, 10) - the
161 master transcription regulators that activate the initial adaptive response to N starvation.
162 However, the absence of either *glnG* (which encodes for NtrC) or *nac* did not detectably affect
163 viability of bacteria under NSIGA or the ability of NSIGA bacteria to recover growth when
164 inoculated into fresh N replete minimal growth media (Fig. 2D and 2E). Overall, we conclude
165 that the transcriptome of *E. coli* during the NAP is dynamic, and this is consistent with the
166 finding above that Rif treatment during the NAP has a detrimental effect on the viability of the
167 *E. coli* population under NSIGA and its ability to recover growth when N becomes replenished.
168 However, it seems that the adaptive transcriptional changes that occur during the NAP happen
169 subsequently to the initial adaptive changes to NISGA and hence do not depend on NtrC (and
170 Nac), which coordinates the initial adaptive transcriptional response to NSIGA.
171
172 **Four upregulated NAP genes are important for optimal growth recovery from**
173 **NSIGA.** We next investigated how the upregulated NAP genes affected viability under NSIGA
174 and growth recovery from NSIGA. Of the 51 51 upregulated NAP genes 44 are available in
175 the Keio single gene knockout collection (11). Thus, we determined how the absence of any of

176 the upregulated NAP genes affected growth recovery from NSIGA. To do this, we grew the
177 library of upregulated NAP gene mutant bacteria in minimal growth media containing excess
178 (10 mM) ammonium chloride as the sole N source and measured cell density after 16 h of
179 growth. The growth of the library of upregulated NAP gene mutant strains was done in a plate
180 reader incubator which allowed continuous monitoring of growth of each mutant strain
181 simultaneously to allow better side-by-side comparison. The results shown in Fig. 3A indicate
182 that absence of any of the NAP genes did not markedly affect growth under N replete
183 conditions. However, we cannot exclude the possibility that the relative dynamics of growth of
184 the individual mutant strains could have differed from that of the wild-type (WT) strain over
185 the 16 h period of time. We note that bacteria in which the tryptophan biosynthesis genes are
186 deleted, lack γ subunit of formate dehydrogenase-N (*fdnI*) or ferric rhodotorulic acid outer
187 membrane transporter (*fhuE*), are unable to grow in our minimal growth media, most likely
188 due to auxotrophy (12). Next, we reinoculated bacteria that grew under N replete conditions
189 into fresh minimal growth media containing limiting, i.e. 3 mM, ammonium chloride and
190 determined how the absence of the upregulated NAP genes affected viability at N-24, i.e.
191 following 24 h under NSIGA. The results in Fig. 3B show that the viabilities of the upregulated
192 NAP gene mutants were similar to that of the WT strain. However, when the 24 h N starved
193 mutant bacteria were inoculated into fresh N replete minimal growth media, the dynamics of
194 growth recovery for the majority of the mutant strains were similar to that of the WT strain
195 (Fig. 3C). However, Δ*allB*, Δ*leuO*, Δ*ynfP*, and Δ*ybcJ* mutant strains displayed noticeably
196 compromised growth recovery properties compared to that of the WT strain (Fig. 3C). These
197 genes encode an allantoinase (*allB*), a DNA-binding transcription dual regulator (*leuO*), a
198 small, possibly fragmented, protein of unknown function (*ynfP*), and a putative RNA-binding
199 protein (*ybcJ*) (12). As shown in Fig. 3D, although the doubling time of Δ*allB*, Δ*leuO*, Δ*ynfP*,
200 and Δ*ybcJ* mutant strains were similar to that of the WT strain, their lag time to growth recovery

201 was increased by ~1.5-4 h compared to that of the WT strain. Thus, it seems that the
202 transcription of *allB*, *leuO*, *ynfP*, and *ybcJ* during the NAP are required for optimal growth
203 recovery from NSIGA. As the Δ*allB* mutant strain displayed the most pronounced
204 compromised ability to recover growth (Fig. 3C) when compared to the WT strain, we decided
205 to focus on the role of *allB* during the NAP and recovery from NSIGA.
206
207 **The degradation of allantoin during the NAP is required for optimal growth**
208 **recovery from NSIGA.** To discount the possibility that the difference in lag time during
209 growth recovery between the WT and Δ*allB* bacteria was not due to the presence of a
210 subpopulation of slow growing Δ*allB* bacteria, we measured the lag time distribution of
211 appearance of individual colonies during growth recovery using ScanLag (7) as described in
212 Fig. 1E. As shown in Fig. 4A, we observed the expected lag time in growth recovery for the
213 Δ*allB* bacteria, but no evidence of a slow growing subpopulation was seen. Further, we did
214 not detect a lag in growth recovery of WT and Δ*allB* bacteria sampled from N- when
215 reinoculated into N replete fresh growth medium (Fig. 4B). This result underscores the view
216 that *allB* has a specific role in *E. coli* during the NAP. To establish that the increased lag time
217 in growth recovery of Δ*allB* bacteria was directly due to the absence of *allB*, we complemented
218 the Δ*allB* bacteria with plasmid-borne *allB*. As shown in Fig. 4C and 4D, the lag time in growth
219 recovery of Δ*allB* bacteria reverted to that of WT bacteria when *allB* was supplied via a
220 plasmid. The product of *allB* is allantoinase, a tetrameric enzyme that catalyses the hydrolytic
221 conversion of (*S*)-(+)-allantoin to allantoate. A previous study (13) reported that substitutions
222 at invariant amino acid positions N94 and S317 (in both cases to D and V), which are located
223 proximal to the active centre, rendered allantoinase inactive (Fig. 4E). As shown in Fig. 4C
224 and 4D, in the context of the complementation experiments, plasmid-borne *allB*-N94V and
225 *allB*-S317V failed to fully decrease the lag time in growth recovery of Δ*allB* bacteria as seen

226 with the WT version of *allB*. In contrast, plasmid-borne *allB*-N94D and to a larger extent *allB*-
227 S317D reverted the lag time in growth recovery of Δ*allB* bacteria as seen with the WT version
228 of *allB*. Although we are unable to explain why specifically substitution by D but not V at N94
229 or S317 renders allantoinase catalytically inactive under our experimental conditions, it seems
230 that the degradation of allantoin occurs at some point in *E. coli* experiencing NSIGA. This is
231 conceivable because, as shown in Fig. 4F, the conversion of allantoate (the product of
232 allantoinase) to S-ureidoglycine by allantoate amidohydrolase (AllC) and the subsequent
233 conversion of (*S*)-ureidoglycine to (S)-ureidoglycolate by (*S*)-ureidoglycine aminohydrolase
234 (AllE) produces ammonium, which may be needed for maintenance of cellular functions
235 required for optimal growth recovery from NSIGA. Consistent with this view, we observed
236 that 24 h N starved Δ*allC* and Δ*allE* bacteria displayed a similarly increased lag time to growth
237 recovery as the Δ*allB* bacteria (Fig. 4G and 4H) when grown in fresh N replete growth media.
238 As allantoin is a product of the purine degradation pathway in N starved *E. coli* (14), we
239 considered whether the requirement for *allB* is a consequence of purine degradation in *E. coli*
240 during the NAP. In other words, we considered whether purines are degraded to replenish
241 diminishing N sources during the NAP to sustain cellular functions via the allantoin
242 degradation pathway (as in Fig. 4F). To indirectly determine whether purines are degraded in
243 *E. coli* during the NAP, we measured the integrity of total RNA as a surrogate for purine
244 degradation in *E. coli* as a function of time in the NAP by chip-based capillary electrophoresis
245 (see Materials and Methods). As shown in Fig. 4J, strikingly, we observed a gradual
246 degradation of 16S and 23S ribosomal RNA as the NAP ensued. This observation further
247 underscores the view that RNA landscape and turnover during the NAP is plastic and consistent
248 with the view that the transcriptome of *E. coli* under NSIGA is dynamic. Collectively, the
249 results are support the view that *allB* contributes to optimal growth recovery from NSIGA by

250 the degradation of allantoin during the NAP in *E. coli*, which most probably accumulates as a
251 result of purine degradation.
252
253 **CONCLUSIONS**
254
255 N is central to all metabolic process in the bacterial cell. As such, bacteria can utilize a wide
256 range of N containing compounds as sole sources of cellular N. Upon N run-out, *E. coli* cells
257 activate the transcription of genes associated with N assimilatory metabolic pathways
258 necessary for utilization of N from the extracellular environment and catabolic biosynthetic
259 pathways for intracellular assimilation of N. We have presented evidence that the growth a
260 population of N starved *E. coli* does not completely cease upon N run-out and that *E. coli* are
261 transcriptionally active for a period of up to 24 h – the NAP - following entry into NSIGA. It
262 seems that NAP represents an important adaptive phase in *E. coli* experiencing NSIGA to
263 maximise chances of viability and optimise growth recovery should N become replenished.
264 We have also presented evidence that the adaptive transcriptional response to NSIGA in *E. coli*
265 during the NAP occurs in at least two distinct temporally coordinated phases: The NtrC
266 dependent initial response to NSIGA is followed by – to a large extent – a NtrC independent
267 transcriptional response. We have uncovered that an aspect of the adaptive transcriptional
268 response that occurs in the NAP subsequent to the initial adaptive transcription response in *E.*
269 *coli* under NSIGA involves the degradation of allantoin. As ammonium is a by-product of
270 degradation of allantoin, we propose that allantoin degradation allows the assimilation of
271 ammonium into glutamine and glutamate to maintain cellular processes during the NAP to
272 maximise chances of viability and optimise growth recovery when N becomes replenished.
273 Previous studies have shown that allantoin can *only* be used as the sole N source by *E. coli*
274 grown under anaerobic conditions (15, 16), and consistent with these results, we were unable

275 to grow Δ*allB* and WT bacteria under our conditions when ammonium chloride (the sole N
276 source used in our experiments) was replaced by allantoin - in both, the initial growth and
277 recovery growth experiments (data not shown). Therefore, as the end-product of allantoin
278 degradation under aerobic conditions is 3-phosphoglycerate, in addition to the by-product
279 ammonium, we propose that the breakdown of allantoin, which likely occurs as a consequence
280 of purine catabolism during the NAP in *E. coli* under NSIGA, serves to maintain as some sort
281 of 'metabolic threshold' to allow optimal growth recovery of *E. coli* from NSIGA under
282 aerobic conditions when N becomes replenished. Although future work will focus on
283 deciphering the metabolic landscape to unravel the metabolic adaptive responses that define
284 the NAP in *E. coli* under NSIGA, this work has underscored the importance of studying the
285 transcriptional changes that occur in growth attenuated bacteria to further our understanding of
286 bacterial stress physiology.
287
288 **MATERIALS AND METHODS**
289 **Bacterial strains and plasmids, growth conditions and viability measurements.**
290 WT and mutant *E. coli* BW25113 strains were used in this study (11). Bacteria were grown as
291 described in Figueira et al (17) in 10 mM NH_4Cl (for overnight cultures) or 3 mM NH_4Cl (for
292 inducing NSIGA) Gutnick minimal medium, consisting of 33.8 mM KH_2PO_4 , 77.5 mM
293 K_2HPO_4 , 5.74 mM K_2SO_4 , 0.41 mM $MgSO_4$, supplemented with Ho-LE trace elements and
294 0.4 % (w/v) glucose, using NH_4Cl as the sole N source (9). Where relevant, rifampicin was
295 added at a final concentration of 150 µg/ml at N-1 or N+ as stated, and L-arabinose was added
296 to complementation strains containing the pBAD18 plasmid at 0.2% (w/v) for induction of
297 gene expression in growth cultures. Ampicillin was added at a final concentration of 100 µg/ml
298 to all cultures containing derivatives of the pBAD18 plasmid. Measurement of growth was
299 taken by measuring the optical density (OD_{600nm}) of bacterial cultures over time to generate

300 growth curves. To determine population viability, the number of viable cells was calculated by
301 conducting serial dilutions of cultures at designated time points as shown in relevant figures,
302 grown overnight on Luria-Bertani (LB) agar plates, and measuring colony forming units (c.f.u.)
303 per ml. The pBAD18-*allB* plasmid was made by traditional restriction enzyme cloning to
304 incorporate the ribosomal binding site of pET33b(+) with the *allB* gene to allow arabinose-
305 inducible expression of the AllB protein. The N94D, N94V, S317D and S317V mutations in
306 *allB* were done by standard site-directed mutagenesis using pBAD18-*allB* as the template.

307 **ScanLag**. Bacteria we grown in 3 mM Gutnick minimal medium to N-24, washed twice
308 in 1 ml PBS, and diluted in PBS. One hundred microlitres of diluted culture was spread on an
309 LB agar plate and incubated at 33 °C for 48 h with pictures of plates taken every 20 minutes.
310 Analysis of colony growth rate and appearance time was modified from Levin-Reisman et al
311 (18) by Dr Miles Priestman and is available at
312 https://github.com/mountainpenguin/NQBMatlab.

313 **RNA-sequencing (RNA-seq).** The RNA-seq data set was previously generated and
314 analysed by Switzer et al (8). The analysis of differential gene expression during NAP as well
315 as the statistical analyses were also conducted in the same way as described previously. The
316 sequencing data can be accessed under accession number E-MTAB-6491 in the ArrayExpress
317 database at EMBL-EBI (www.ebi.ack.uk/arrayexpress).

318 **Total RNA analysis.** Cultures were grown as above and sampled at the following time
319 points: at the onset of N starvation (N-) and 3 h (N-3), 6 h (N-6), 9 h (N-9), 12 h (N-12), 18 h
320 (N-18), and 24 h (N-24) under N starvation. At least three biological replicates were taken at
321 each time point. RNA was acquired and stabilized at specified time points using Qiagen RNA
322 Protect reagent (Qiagen, 76526). RNA extraction was carried out using the PureLink RNA
323 mini kit (Invitrogen, 12183025) and DNase Set (Invitrogen, 12185010) as per manufacturer's
324 protocol. Electropherograms of total RNA integrity were generated using an Agilent

325 Bioanalyser 2100 instrument (Agilent, G2939BA) and RNA 6000 Nano kit (Agilent, 5067-
326 1511) as per the manufacturer's protocol.

327 **Statistical analysis and growth calculations.** Unless otherwise stated in the text, all
328 growth curves and c.f.u. data show the mean average of three independent experiments and
329 variation calculated by the standard error of the mean (SEM). The student's t-test or one-way
330 ANOVA was used to determine statistical significance if the probability (*P*) value was < 0.05
331 (* $P < 0.05$, ** $P < 0.01$, *** $P < 0.001$). Lag and doubling times were calculated by first
332 generating a straight-line graph of the exponential growth section of each growth curve. Lag
333 time was defined as the intersection of the straight line graph with the x axis, while the doubling
334 time was determined during exponential growth (19).

335

336 **FIGURE LEGENDS**

337

338 **Fig 1. Perturbation of the transcriptional response during NSIGA compromises survival**
339 **and growth recovery of *E. coli*.** (A) Graph showing viability, measured by counting colony
340 forming units (c.f.u.) of *E. coli* over 5 days under NSIGA. Inset table shows doubling time
341 between different growth periods. (B) Graph showing proportion of viable cells (measured by
342 c.f.u.) in the population of *E. coli* under NSIGA with (red) and without (blue) Rif treatment at
343 N-1; the dashed red line indicates addition of Rif to N+ cells (see text for details). (C) Graph
344 showing recovery growth in fresh N replete medium as measured by OD_{600nm} readings. The
345 time points and conditions from which bacteria were sampled for recovery growth experiments
346 are indicated and discussed in the text. (D) Graph showing lag time and doubling time during
347 growth recovery experiments from (C). (E) ScanLag analysis of colony growth rate and
348 appearance time after plating of 24 h N starved bacteria on LB agar after Rif treatment (red)
349 and no Rif treatment (blue) at N-1. The various shades of the same colour represent distinct

350 biological replicates, where n=3. In (A)-(D), error bars represent SEM, where n=3 and the
351 schematics describe the different experiments for ease of understanding.
352
353 **Fig 2. The transcriptome of NSIGA *E. coli* is dynamic.** (A) Graphs showing the $\log_2$ fold
354 change in gene expression at N- compared to N+ (Phase A), and N-24 compared to N- (Phase
355 B). Genes in blue (Phase A) or red (Phase B = NAP) represent significant differential
356 expression above a $\log_2$ fold change of 1 and a false discovery rate adjusted P value < 0.05.
357 Genes in black (Phase B) represent the NAP genes, defined as having significant differential
358 gene expression unique to Phase B (NAP), but not Phase A. (B) Venn diagrams showing genes
359 significantly upregulated (top) and downregulated (bottom) in Phase A compared to Phase B.
360 (C) Graph showing Clusters of Orthologous Groups (COG) categorisation of NAP genes, and
361 the number of genes within each category whose expression is up- or downregulated from N-.
362 (D) Graph showing viability as measured by c.f.u. counting of viable cells in the population of
363 WT (blue), Δ*glnG* (red) and Δ*nac* (green) bacteria over 48 h of N starvation (*left*). Graph
364 showing growth recovery of N-24 WT (blue), Δ*glnG* (red) and Δ*nac* (green) bacteria in N
365 replete fresh media as measured by OD_{600nm} readings. In both graphs, error bars represent SEM,
366 where n=3.
367
368 **Fig 3. Four upregulated NAP genes are important for optimal growth recovery from**
369 **NSIGA.** (A) Graph showing overnight growth of NAP gene mutant bacteria as measured by
370 OD_{600nm} compared to WT (blue) bacteria in minimal growth media containing excess (10 mM)
371 N (ammonium chloride). (B) Graph showing viability as measured by c.f.u. counts of wild-
372 type (blue) and NAP gene mutant bacteria (black) bacteria at N-24. (C) Graph showing
373 recovery growth of 24 h N starved NAP gene mutant bacteria in N replete fresh media as
374 measured by OD_{600nm} readings. The recovery growth curves of WT (blue), Δ*allB* (red), Δ*leuO*

375 (dark green), Δ*ynfP* (purple), and Δ*ybcJ* (orange) are highlighted. (D) Graph showing lag time
376 (blue) and doubling time (red) of WT, Δ*allB*, Δ*leuO*, Δ*ynfP*, and Δ*ybcJ* bacteria extracted from
377 the growth curves in (C). In (C) and (D), the error bars represent SEM, where *n*=2. Statistical
378 analyses were performed using the Student's *t*-test (**P* < 0.05, ***P* < 0.01).
379
380 **Fig. 4. The degradation of allantoin during the NAP is required for optimal growth**
381 **recovery from NSIGA.** (A) ScanLag analysis of colony growth rate and appearance time after
382 plating of 24 h N starved WT (blue) and Δ*allB* (red) bacteria on LB agar. Various shades of
383 the same colour represent distinct biological replicates, where n=3. (B) Graph showing the
384 recovery growth curves of WT (blue) and Δ*allB* (red) bacteria from the onset of N starvation
385 (N-) in fresh N replete media as measured by OD_{600nm} readings of the cultures. (C) Graph
386 showing the recovery growth curves of 24 h N starved WT + pBAD18 (blue), Δ*allB* + pBAD18
387 (red), and Δ*allB* + pBAD18-*allB* (green) bacteria in fresh N replete media as measured by
388 OD_{600nm} readings of the cultures. (D) Graph showing lag time to growth recovery of WT +
389 pBAD18 (blue), Δ*allB* + pBAD18 (red), Δ*allB* + pBAD18-*allB* (bright green), Δ*allB* +
390 pBAD18-*allB* N94D, Δ*allB* + pBAD18-*allB* N94V, Δ*allB* + pBAD18-*allB* S317D and Δ*allB*
391 + pBAD18-*allB* S317V in fresh N replete media as extracted by OD_{600nm} readings of the
392 cultures. (E) Cartoon representation of the structure of a monomer of AllB in which the
393 positions of the N94 and S317 are indicated in orange relative to the two Fe moieties at the
394 active site of the enzyme (indicated in red). (F) A schematic showing the allantoin degradation
395 pathway indicating the steps where ammonia is produced. (G) As in (C), but the experiment
396 was conducted with Δ*allC* and Δ*allE* bacteria. (H) Graph showing lag time (blue) and doubling
397 time (red) of WT, Δ*allB*, Δ*allC* and Δ*allE* bacteria extracted from the growth curves in (G). (I)
398 Electropherogram of total RNA from bacterial cultures taken at indicated timepoints. Graph

399 shows representative data from at least three biological replicates. 16S and 23S rRNA peaks

400 are indicated. In (B), (C), (D), (G) and (H) error bars represent SEM, where n=3.

401

402 **ACKNOWLEDGMENTS**

403 A Wellcome Trust Investigator award WT100958MA and a Leverhulme Trust project grant

404 (RPG-2017-431) funded this work. J. M. is an MRC funded PhD student.

405

406 **REFERENCES**

407 1. Gefen O, Fridman O, Ronin I, Balaban NQ. 2014. Direct observation of single
408 stationary-phase bacteria reveals a surprisingly long period of constant protein
409 production activity. Proc Natl Acad Sci U S A 111:556-61.
410 2. Stapels DAC, Hill PWS, Westermann AJ, Fisher RA, Thurston TL, Saliba AE,
411 Blommestein I, Vogel J, Helaine S. 2018. Salmonella persisters undermine host
412 immune defenses during antibiotic treatment. Science 362:1156-1160.
413 3. Manina G, Dhar N, McKinney JD. 2015. Stress and host immunity amplify
414 Mycobacterium tuberculosis phenotypic heterogeneity and induce nongrowing
415 metabolically active forms. Cell Host Microbe 17:32-46.
416 4. Gray DA, Dugar G, Gamba P, Strahl H, Jonker MJ, Hamoen LW. 2019. Extreme
417 slow growth as alternative strategy to survive deep starvation in bacteria. Nat
418 Commun 10:890.
419 5. Brown DR, Barton G, Pan Z, Buck M, Wigneshweraraj S. 2014. Nitrogen stress
420 response and stringent response are coupled in Escherichia coli. Nat Commun 5:4115.
421 6. Zimmer DP, Soupene E, Lee HL, Wendisch VF, Khodursky AB, Peter BJ, Bender
422 RA, Kustu S. 2000. Nitrogen regulatory protein C-controlled genes of Escherichia
423 coli: scavenging as a defense against nitrogen limitation. Proc Natl Acad Sci U S A
424 97:14674-9.
425 7. Levin-Reisman I, Fridman O, Balaban NQ. 2014. ScanLag: high-throughput
426 quantification of colony growth and lag time. J Vis Exp doi:10.3791/51456.
427 8. Switzer A, Evangelopoulos D, Figueira R, de Carvalho LPS, Brown DR,
428 Wigneshweraraj S. 2018. A novel regulatory factor affecting the transcription of
429 methionine biosynthesis genes in Escherichia coli experiencing sustained nitrogen
430 starvation. Microbiology 164:1457-1470.
431 9. Brown DR, Barton G, Pan Z, Buck M, Wigneshweraraj S. 2014. Combinatorial stress
432 responses: direct coupling of two major stress responses in Escherichia coli. Microb
433 Cell 1:315-317.
434 10. Aquino P, Honda B, Jaini S, Lyubetskaya A, Hosur K, Chiu JG, Ekladious I, Hu D,
435 Jin L, Sayeg MK, Stettner AI, Wang J, Wong BG, Wong WS, Alexander SL, Ba C,
436 Bensussen SI, Bernstein DB, Braff D, Cha S, Cheng DI, Cho JH, Chou K, Chuang J,
437 Gastler DE, Grasso DJ, Greifenberger JS, Guo C, Hawes AK, Israni DV, Jain SR,
438 Kim J, Lei J, Li H, Li D, Li Q, Mancuso CP, Mao N, Masud SF, Meisel CL, Mi J,
439 Nykyforchyn CS, Park M, Peterson HM, Ramirez AK, Reynolds DS, Rim NG, Saffie

JC, Su H, Su WR, et al. 2017. Coordinated regulation of acid resistance in Escherichia coli. BMC Syst Biol 11:1.

11. Baba T, Ara T, Hasegawa M, Takai Y, Okumura Y, Baba M, Datsenko KA, Tomita M, Wanner BL, Mori H. 2006. Construction of Escherichia coli K-12 in-frame, single-gene knockout mutants: the Keio collection. Mol Syst Biol 2:2006 0008.
12. Keseler IM, Mackie A, Santos-Zavaleta A, Billington R, Bonavides-Martinez C, Caspi R, Fulcher C, Gama-Castro S, Kothari A, Krummenacker M, Latendresse M, Muniz-Rascado L, Ong Q, Paley S, Peralta-Gil M, Subhraveti P, Velazquez-Ramirez DA, Weaver D, Collado-Vides J, Paulsen I, Karp PD. 2017. The EcoCyc database: reflecting new knowledge about Escherichia coli K-12. Nucleic Acids Res 45:D543-D550.
13. Kim K, Kim MI, Chung J, Ahn JH, Rhee S. 2009. Crystal structure of metal-dependent allantoinase from Escherichia coli. J Mol Biol 387:1067-74.
14. Xi H, Schneider BL, Reitzer L. 2000. Purine catabolism in Escherichia coli and function of xanthine dehydrogenase in purine salvage. J Bacteriol 182:5332-41.
15. Rintoul MR, Cusa E, Baldoma L, Badia J, Reitzer L, Aguilar J. 2002. Regulation of the Escherichia coli allantoin regulon: coordinated function of the repressor AllR and the activator AllS. J Mol Biol 324:599-610.
16. Cusa E, Obradors N, Baldoma L, Badia J, Aguilar J. 1999. Genetic analysis of a chromosomal region containing genes required for assimilation of allantoin nitrogen and linked glyoxylate metabolism in Escherichia coli. J Bacteriol 181:7479-84.
17. Figueira R, Brown DR, Ferreira D, Eldridge MJ, Burchell L, Pan Z, Helaine S, Wigneshweraraj S. 2015. Adaptation to sustained nitrogen starvation by Escherichia coli requires the eukaryote-like serine/threonine kinase YeaG. Sci Rep 5:17524.
18. Levin-Reisman I, Gefen O, Fridman O, Ronin I, Shwa D, Sheftel H, Balaban NQ. 2010. Automated imaging with ScanLag reveals previously undetectable bacterial growth phenotypes. Nat Methods 7:737-9.
19. Powell EO. 1956. Growth rate and generation time of bacteria, with special reference to continuous culture. J Gen Microbiol 15:492-511.

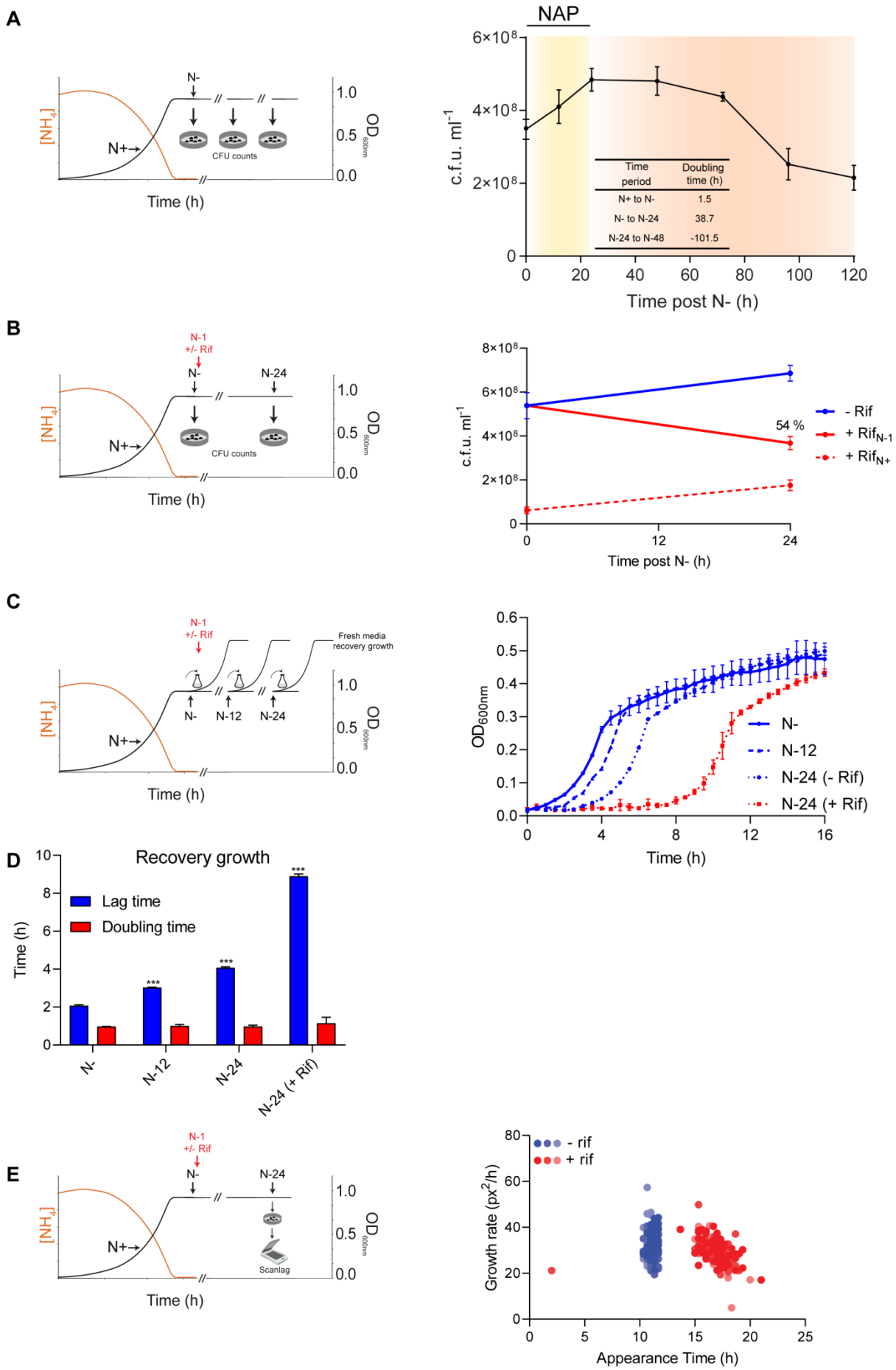
A
N-
N+
CFU counts
[NH4]
OD600nm
Time (h)
NAP
c.f.u. ml-1
Time post N- (h)
Time period
Doubling time (h)
N+ to N-
1.5
N- to N-24
38.7
N-24 to N-48
-101.5
B
N-1
+/- Rif
N-24
54 %
- Rif
+ RifN-1
+ RifN+
C
Fresh media recovery growth
N-12
OD600nm
N-
N-24 (- Rif)
N-24 (+ Rif)
D
Recovery growth
Lag time
Doubling time
N-24 (+ Rif)
E
Scanlag
- rif
+ rif
Growth rate (px2/h)
Appearance Time (h)

Figure 1

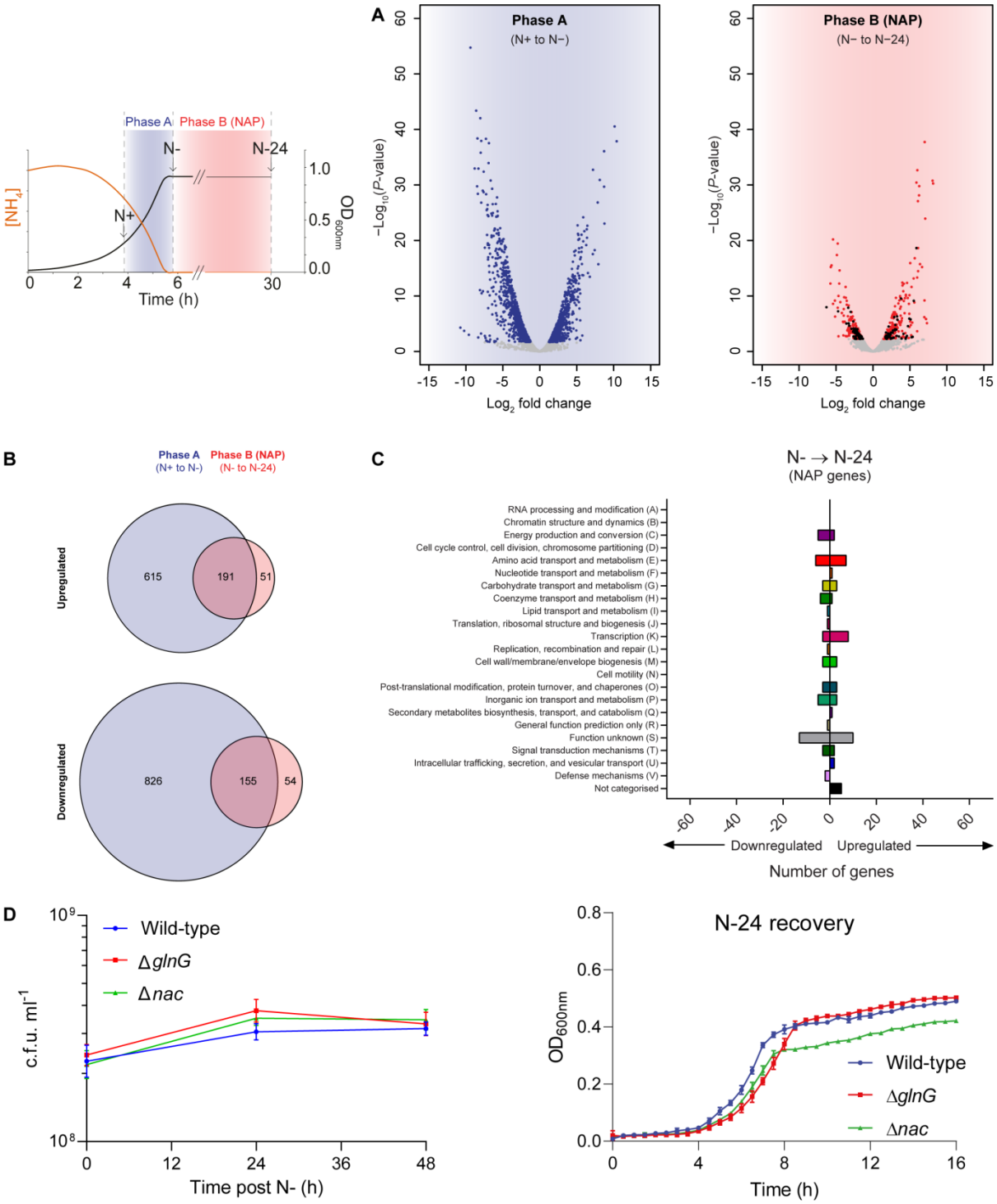
Phase A
Phase B (NAP)
N-
N-24
N+
[NH4]
OD600nm
Time (h)
A
Phase A
(N+ to N−)
Phase B (NAP)
(N− to N−24)
−Log10(P-value)
Log2 fold change
B
Phase A
(N+ to N-)
Phase B (NAP)
(N- to N-24)
Upregulated
615
191
51
Downregulated
826
155
54
C
N- → N-24
(NAP genes)
RNA processing and modification (A)
Chromatin structure and dynamics (B)
Energy production and conversion (C)
Cell cycle control, cell division, chromosome partitioning (D)
Amino acid transport and metabolism (E)
Nucleotide transport and metabolism (F)
Carbohydrate transport and metabolism (G)
Coenzyme transport and metabolism (H)
Lipid transport and metabolism (I)
Translation, ribosomal structure and biogenesis (J)
Transcription (K)
Replication, recombination and repair (L)
Cell wall/membrane/envelope biogenesis (M)
Cell motility (N)
Post-translational modification, protein turnover, and chaperones (O)
Inorganic ion transport and metabolism (P)
Secondary metabolites biosynthesis, transport, and catabolism (Q)
General function prediction only (R)
Function unknown (S)
Signal transduction mechanisms (T)
Intracellular trafficking, secretion, and vesicular transport (U)
Defense mechanisms (V)
Not categorised
Downregulated
Upregulated
Number of genes
D
Wild-type
ΔglnG
Δnac
c.f.u. ml-1
Time post N- (h)
N-24 recovery
OD600nm
Time (h)

Figure 2

503

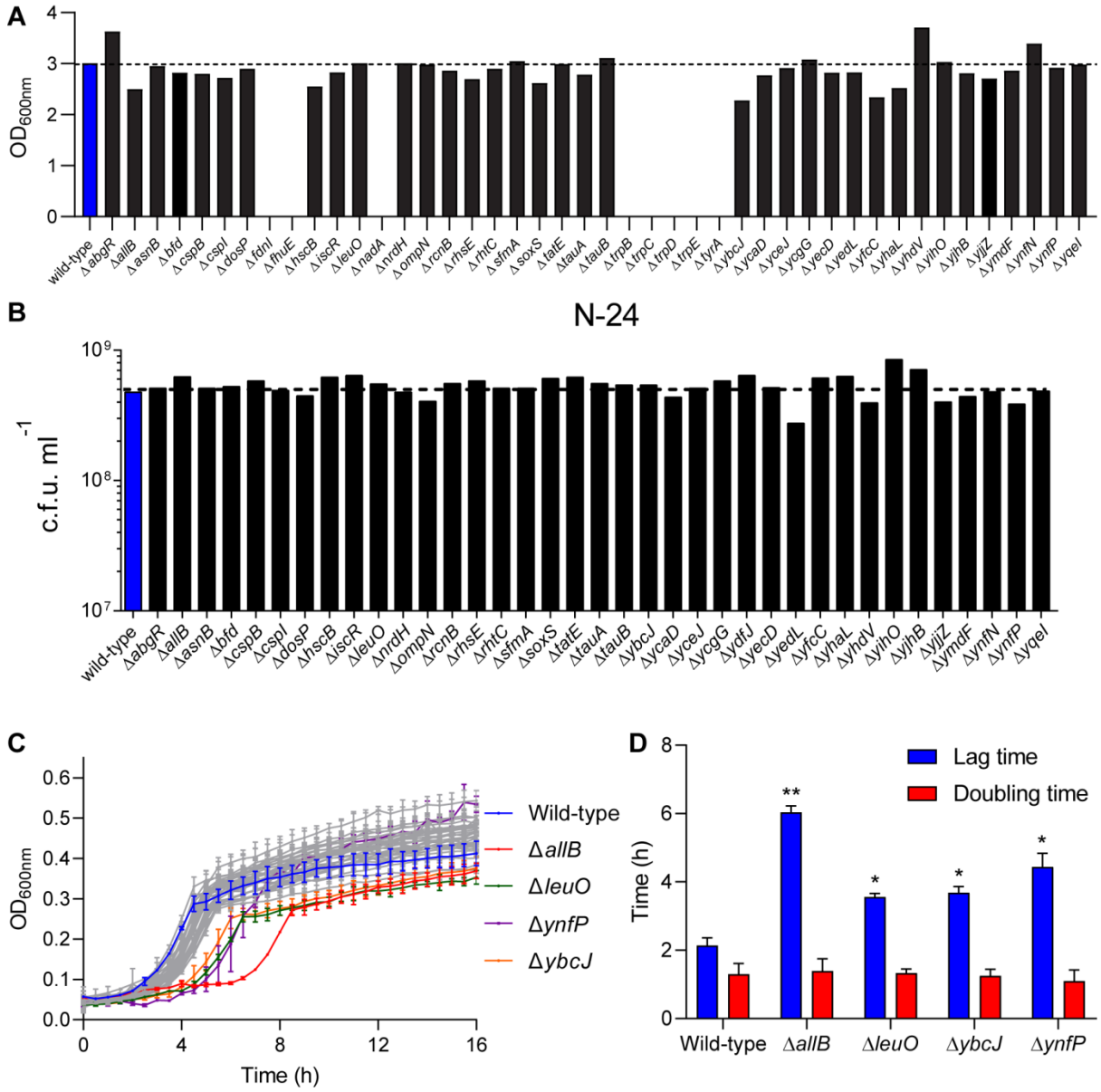

504
505
506
507
508

Figure 3

509
510
511
512
513
514
515
516
517

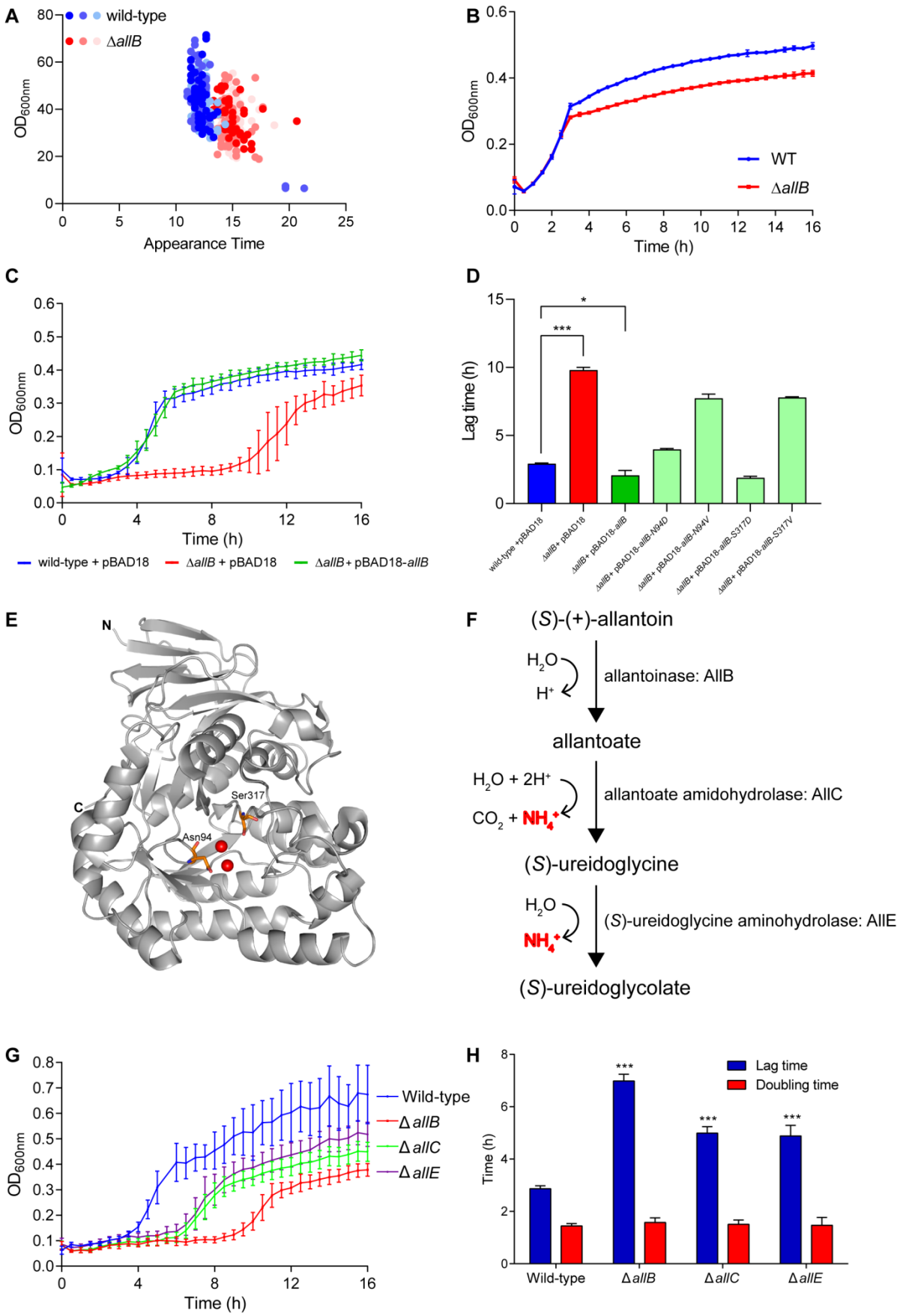
A
wild-type
ΔallB
OD600nm
Appearance Time
B
OD600nm
WT
ΔallB
Time (h)
C
OD600nm
Time (h)
wild-type + pBAD18
ΔallB + pBAD18
ΔallB + pBAD18-allB
D
Lag time (h)
wild-type +pBAD18
ΔallB+ pBAD18
ΔallB+ pBAD18-allB
ΔallB+ pBAD18-allB-N94D
ΔallB+ pBAD18-allB-N94V
ΔallB+ pBAD18-allB-S317D
ΔallB+ pBAD18-allB-S317V
E
N
C
Ser317
Asn94
F
(S)-(+)-allantoin
H2O
H+
allantoinase: AllB
allantoate
H2O + 2H+
CO2 + NH4+
allantoate amidohydrolase: AllC
(S)-ureidoglycine
H2O
NH4+
(S)-ureidoglycine aminohydrolase: AllE
(S)-ureidoglycolate
G
OD600nm
Time (h)
Wild-type
ΔallB
ΔallC
ΔallE
H
Time (h)
Lag time
Doubling time
Wild-type
ΔallB
ΔallC
ΔallE

Figure 4

I

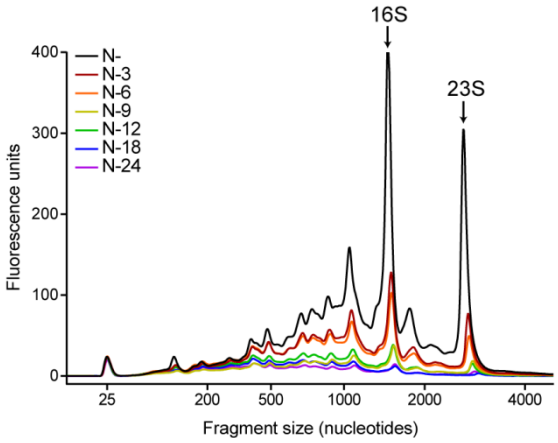

Figure 4 – cont.